Evolution of Epicardial Rotors into Breakthrough Waves during Atrial Fibrillation in 3D Canine Biatrial Model with Detailed Fibre Orientation

Ataollah Tajabadi[1,2], Aditi Roy[1,3], Marta Varela[1,4], Oleg Aslanidi[1]

[1]King's College London, London, United Kingdom
[2]University of Glasgow, Glasgow, United Kingdom
[3]University of Oxford, Oxford, United Kingdom
[4]Imperial College London, London, United Kingdom

Abstract

Atrial fibrillation (AF) is the most common arrhythmia, but its mechanisms are still unclear. Commonly observed phenomena during AF are epicardial re-entrant drivers (rotors) and breakthrough waves. This study aims to elucidate AF mechanisms, including links between rotors and breakthroughs. We used 3D canine atrial models based on micro-CT reconstruction of biatrial geometry combined with region-specific electrophysiology models. Hence, the 3D model included ionic and structural heterogeneities in the entire atria, with special focus on the right atrium (RA) and pectinate muscles (PM). Results were visualized through 3D atrial membrane voltage maps (VM), 2D isochronal maps (IM), and wave maps (WM). AF episodes were initiated in the atria and were maintained by several epicardial rotors in the PV and RA. Transmural rotors were also seen to propagate through the PM and re-emerge at the RA epicardium during these episodes. IM and WM revealed multiple breakthroughs at the region where the PM connect to the RA. The VM simulations, as well as electrogram-based IM and WM, showed that the complex AF patterns seen experimentally can be explained by the interactions of epicardial and transmural rotors.

1.   Introduction

Atrial fibrillation (AF) is a common form of cardiac arrhythmia characterized by the rapid and irregular electrical activation and contraction of the atria. AF can occur as a consequence of a range of conditions including genetic factors, obesity and hypertension [1]. It is theorized that atrial dilation and/or pressure increase associated with such disorders lead to AF, but the understanding of its exact mechanisms is still incomplete [2]. AF is currently understood to be sustained by either a few stable localised rotors, meandering evanescent rotors anchored to fibrotic borders, or multiple breakthroughs waves originating from an epicardial-endocardial dissociation. These numerous contending observations have created debate regarding the primary source of AF [3]. The exact mechanisms of AF can significantly impact therapies like anti-arrhythmic drugs and ablation, as success of the procedures is dependent upon eliminating the source. This study aims to show that rotors evolve into breakthroughs via the formation of a 'transmural rotor' that propagates through the atrial volume via the pectinate muscles (PMs). The right atrium (RA) has a branched network of PMs that are mechanically tasked with the aiding blood flow [4], and so must be electrically synchronized with the surrounding tissue. A disruption of this harmony may create a highway capable of guiding and maintaining transmural rotors, which subsequently disturb the functional dynamics of the atria.

2.   Methods

Our study uses a 3D reconstruction of the canine atria; however, the human atria are structurally and functionally similar, and the simulation results can be used to explain the respective mechanisms in human AF. The 3D atrial geometry was obtained by semi-automatic segmentation of micro-computed tomography (micro-CT) atrial images [5]. The resolution was reduced from 36 μm to 300 μm to improve computational efficiency [6,7]. The geometry was segmented into 5 regions (Fig. 1): RA, PMs, left atrium (LA), Bachmann's bundle-cristae terminalis (BB-CT) and pulmonary veins (PVs). Cardiac muscle fibre (myofiber) orientation was also incorporated as its arrangement greatly influences the distribution of electrical signals across the tissue due to its anisotropic electrical properties.

Mathematically, the change in transmembrane voltage (V_m) over a volume is described by equation (1):

$$\frac{\partial V_m}{\partial t} = \nabla \cdot \left(\widetilde{D} \nabla V_m \right) - \frac{I_{ion}}{C_m} \qquad \widetilde{D} = \begin{pmatrix} D_{\parallel} & 0 & 0 \\ 0 & D_{\perp} & 0 \\ 0 & 0 & D_{\perp} \end{pmatrix} (1)$$

Here, $\widetilde{D}$ is the diffusion tensor, I_{ion} is the transmembrane current per unit area, and C_m is the membrane capacitance. The $\nabla \cdot \left(\widetilde{D} \nabla V_m \right)$ represents the change in V_m due to ion flow from adjacent cells, which controls rate of AP spread throughout the cardiac tissue.

The diagonal components of $\widetilde{D}$ are diffusion coefficients for moving parallel ($D_\parallel$) and perpendicular ($D_\perp$) to the myofibre's long axis. Fibrosis, a condition that is associated with chronic AF, causes significant loss of AP conductivity across fibrotic areas [8]. This was modelled by reducing the diffusion coefficients in those regions.
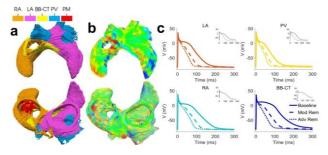

Figure 1. 3D canine atrial geometry (a) with myofibre orientation (b); Epicardial (top) and Endocardial views (bottom) are shown; fibre orientation vectors are coloured according to a component in endocardial direction. (c) Single cell AP morphologies for each region with different degrees of ionic remodelling. Reproduced from [6].

I_{ion} was calculated using either the Fenton-Karma (FK) [9] or Varela et al. models [6]. Parameters of the FK model have been altered to model chronic AF conditions [10]. In the FK simulations, the diffusion coefficient of the LA, RA, BB-CT, and PVs (referred to here as non-PM cells) were set to one value, while the PMs was set to a lower value to mimic the presence of fibrosis in this region [11].

The Varela model was used to better represent the true electrophysiological behaviour of the canine atria. Ionic and structural remodelling, as described by [6], was also implemented into the simulations. Due to absence of data on PM-specific AP, PMs used the same single cell model as the RA; however, the diffusion coefficient values and degrees of ionic remodelling were different to reflect heterogeneity of this region. Various combinations of PM and RA ionic and structural remodelling stages were tested to find the parameters that were able to create stable transmural rotors. AF was initiated by rapid atrial pacing in the PVs that were simulated 4 times at set S_2 intervals. All results were visualised using Paraview (Kitware).

2D isochronal activation maps, which show electrode activation times within a given period, is a popular method for visualising AF voltage patterns. We recorded voltages in the 3D atria every 10 ms for the isochronal maps (IM). Due to the complex nature of simulated AF, it was difficult to separate breakthroughs from rotors using the IM alone. Hence, the waves were segmented into individual wave-fronts to create wave maps (WM). We observed that an AP could only propagate across one electrode in a 10 ms time step, so we created a script that checked each activated electrode and compared its current value with the previous value. If electrode activation corresponded to adjacent

electrode deactivation, then the signal was assumed to have propagated from one electrode to another; otherwise, the activation was attributed to a breakthrough wave. Matlab (Mathworks) was used to simulate the electrograms.

3. Results

Parameters used to generate AF in the FK model are detailed in Table 1. 3D voltage maps at 2460 ms of the simulation show a complex AF episode with a transmural rotor present in the PM (Fig. 2b). A breakthrough wave can be seen where the PM reconnect to the epicardial surface (Fig. 2a); transient epicardial rotors were also observed. Fig. 2 also shows a second path where the rotor travels on the surface moving from the epicardium to endocardium after which it returns to the epicardium through the PMs. 2D IM/WM showed that the single breakthrough seen in the 3D maps was in fact four separate waves (Fig. 2c, 2d). The size of the stars the latter figures is proportional to the number of electrodes that were simultaneously activated by the breakthrough. The epicardial and endocardial maps also show that the origin and time of electrode activation differ between the two layers.

S_2 (ms)	$D_\parallel (mm^2/ms)$; $D_\perp (mm^2/ms)$	$D_\parallel^{PM} (mm^2/ms)$; $D_\perp^{PM} (mm^2/ms)$
105	0.4; 0.0267	0.0067; 0.00044

Table 1. Parameters for the FK simulations: pacing period (S_2), longitudinal and transverse diffusion coefficients for non-PM ($D_\parallel$, $D_\perp$) and PM ($D_\parallel^{PM}$, $D_\perp^{PM}$) regions.
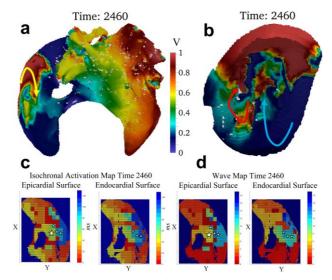

Figure 2. 3D voltage map of the FK model simulation in epicardial (a) and endocardial (b) views. The voltage is normalised and color-coded. Arrows represent surface (yellow) and transmural (red, blue) rotor paths. IM (c) and WM (d) with breakthrough waves (stars) are shown.

Conditions used to generate AF in the Varela model simulations are detailed in Table 2. At 2370 *ms* the simulation showed two localised epicardial rotors at the PVs (Fig. 3a). The RA was characterised with less coherent behaviour and asynchronous activity in the PM region. Upon closer inspection of the 3D voltage dynamics, a transmural rotor was observed in the PMs. Due to the complex behaviour of the AF episode, it was difficult to see obvious breakthrough waves in the 3D voltage maps; however, the 2D electrograms clearly showed the presence of a single breakthrough in both the endocardial and epicardial layers. Similar to the FK model simulations, one transmural rotor moves through a path in the PMs, and another through the endocardial surface (Fig. 3b).

S_2 (*ms*)	Structural Remodelling	Ionic Remodelling
105	Non-PM: CVR	Non-PM: Moderate
	PM: CVR	PM: None

Table 2. Conditions for the Varela model simulation. Parameters are the pacing period (S_2), and degree of structural/ionic remodelling for non-PM and PM cells [6].
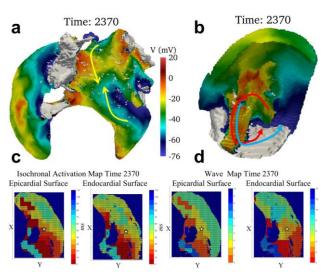
Figure 3. 3D voltage map of the Varela model simulation in epicardial (a) and endocardial (b) views. The voltage is normalised and color-coded. Arrows represent surface (yellow) and transmural (red, blue) rotor paths. IM (c) and WM (d) with breakthrough waves (stars) are shown.

The addition of 10μM Amiodarone to the simulation of AF greatly impacted the number and type of waveforms being sustained. After 9920 *ms* into the simulation, there was neither evidence of surface rotors nor breakthroughs in the RA, and APs propagated in that region as regular quasi-plane waves (Fig. 4). In the PM region, the transmural rotor also disappeared, and APs in epi- and endocardial layers moved cohesively and synchronously. Only a single rotor remained in the PVs.
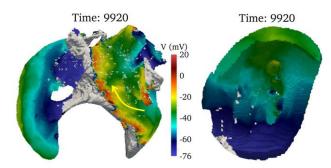
Figure 4. 3D voltage map of the Varela model simulation with amiodarone in the epicardial (left) and endocardial (right) views. Arrow represents the surface rotor path.

4. Discussion

Simulations of electrophysiologically and structurally detailed 3D canine atrial models provided novel insights in the interplay between rotors and breakthrough waves maintaining AF. The latter emerged as a manifestation of transmural rotors propagating from the depth of RA tissue.

In the FK model simulations, a transmural rotor was formed due to the PMs' branched structure combined with the AP velocity reduced due to fibrosis. The transmural rotor either moved strictly through the PMs and reappeared at the RA endocardial surface as breakthrough waves, or exited the PMs and travelled along the surface. Although the latter didn't result in the formation of breakthroughs, its movement disrupted the organised atrial activations and resulted in transient rotors. The Varela model simulations demonstrated the formation of localised rotors in the PVs, in addition to transmural rotors in the PMs. Interaction of transmural rotors with APs incoming from the LA led to transient re-entries in the RA (not shown). The addition of amiodarone to the AF simulations caused the elimination of transmural rotors and breakthrough waves in the RA, with a single rotor remaining in the PVs. This effect can be explained by non-uniform increase of the AP duration by amiodarone, with the shortest AP in the PV region facilitating the re-entrant movement. This is in agreement with the previous results by Varela et al [6]. The current study demonstrated that transmural rotors are not immune to its anti-arrhythmic effects and increasing AP duration is an effective method of preventing their formation.

4.4 Future Work

The mechanism described in this study depends on the presence of heterogeneities between the RA and PMs. While the existence of such heterogeneity is well known, the precise measurements of AP and ionic differences between the regions are limited. Moreover, changes of electrophysiological heterogeneity between the RA and

PMs due to remodelling are poorly documented. Taking these data into account would help provide further insights into the complex 3D dynamics in the atria during AF.

The presence of fibrosis was accounted for in this study as decreases of diffusion coefficients in the entire atria (to mimic slower AP conduction during chronic AF), and further localised decreases in the PM region. More detailed distributions of fibrosis can be reconstructed from MRI and incorporated into the 3D atrial models [12,13].

Finally, complex AF episodes were simulated in this study using canine atrial geometry and electrophysiology. Although canine hearts are structurally and functionally similar to the human ones, using 3D human atrial models will ultimately be needed to confirm the presence of such mechanisms in patients and find ways to treat them [14]. The application of advanced AI methods in combination with the models could help achieve the latter aim [15].

5.   Conclusion

The 3D canine atrial model simulations demonstrated that propagation of transmural rotors through the depth of 3D atrial tissue can appear as breakthroughs on the RA surface, and can also cause further transient re-entries. Simulations of the detailed model by Varela et al. [6] in particular showed multiple drivers for AF to be present simultaneously. These results can reconcile apparently controversial viewpoints on AF mechanisms and potentially improve mechanism-based AF treatments.

Acknowledgments

References

[1]   J. M. B. Anumonwo and J. Kalifa, "Risk Factors and Genetics of Atrial Fibrillation," *Cardiol. Clin.*, vol. 32, pp. 485–494, 2014, doi: 10.1016/j.ccl.2014.07.007.

[2]   S. Nattel, "New ideas about atrial fibrillation 50 years on," *Nature*, vol. 415, no. 6868, pp. 219–226, 2002, doi: 10.1038/415219a.

[3]   S. Nattel and D. Dobrev, "Controversies about Atrial Fibrillation Mechanisms: Aiming for Order in Chaos and Whether it Matters," *Circ. Res.*, vol. 120, no. 9, pp. 1396–1398, 2017, doi: 10.1161/CIRCRESAHA.116.310489.

[4]   A. Keith, "An Account of the Structures concerned in the Production of the Jugular Pulse," *Journal of Anatomy and Physiology*, vol. 42, no. Pt 1. pp. 1–25, Oct. 1907.

[5]   O. V. Aslanidi *et al.*, "Application of Micro-Computed Tomography With Iodine Staining to Cardiac Imaging, Segmentation, and Computational Model Development," *IEEE Trans. Med. Imaging*, vol. 32, no. 1, pp. 8–17, 2013, doi: 10.1109/TMI.2012.2209183.

[6]   M. Varela, M. A. Colman, J. C. Hancox, and O. V. Aslanidi, "Atrial Heterogeneity Generates Re-entrant Substrate during Atrial Fibrillation and Anti-arrhythmic Drug Action: Mechanistic Insights from Canine Atrial Models," *PLoS Comput. Biol.*, vol. 12, no. 12, pp. 1–22, 2016, doi: 10.1371/journal.pcbi.1005245.

[7]   Colman, M., Varela, M., Hancox, J.C., Zhang, H., and Aslanidi, O. Evolution and pharmacological modulation of the arrhythmogenic wave dynamics in canine pulmonary vein model. *Europace*. 16, 416–23, 2014, doi: 10.1371/journal.pcbi.1005245.

[8]   B. Burstein and S. Nattel, "Atrial Fibrosis: Mechanisms and Clinical Relevance in Atrial Fibrillation," *J. Am. Coll. Cardiol.*, vol. 51, no. 8, pp. 802–809, Feb. 2008, doi: 10.1016/J.JACC.2007.09.064.

[9]   F. Fenton and A. Karma, "Vortex dynamics in three-dimensional continous myocardium with fiber rotation: Filament instablity and fibrillation," *Chaos*, vol. 8, no. 1, pp. 20–47, 1998, doi: 10.1063/1.166374.

[10]   A. M. Goodman, R. A. Oliver, C. S. Henriquez, and P. D. Wolf, "A membrane model of electrically remodelled atrial myocardium derived from in vivo measurements," *Europace*, vol. 7, no. SUPPL. 2, pp. S135–S145, Sep. 2005, doi: 10.1016/j.eupc.2005.04.010.

[11]   Hansen, B., *et al*. Atrial fibrillation driven by micro-anatomic intramural re-entry revealed by simultaneous sub-epicardial and sub-endocardial optical mapping in explanted human hearts. *European Heart Journal*, vol. 36, no. 35, pp. 2390–2401, 2015, doi: 10.1093/eurheartj/ehv233.

[12]   Roy, A., Varela, M., and Aslanidi, O. Image-based computational evaluation of the effects of atrial wall thickness and fibrosis on re-entrant drivers for atrial fibrillation. *Front. Physiol.* 9:1352, 2018, doi: 10.3389/fphys.2018.01352.

[13]   Roy, A., Varela, M., Chubb, H., MacLeod, R., Hancox, J. C., Schaeffter, T., Aslanidi, O. Identifying locations of re-entrant drivers from patient-specific distribution of fibrosis in the left atrium. *PLoS Comput. Biol.* 16:e1008086, 2020, doi: 10.1371/journal.pcbi.1008086.

[14]   Boyle, P. M., Zghaib, T., Zahid, S., Ali, R. L., Deng, D., Franceschi, W. H., et al. Computationally guided personalized targeted ablation of persistent atrial fibrillation. *Nat. Biomed. Eng.* 3, 870–879, 2019, doi: 10.1038/s41551-019-0437-9.

[15]   Muffoletto, M., Qureshi, A., Zeidan, A., Muizniece, L., Fu, X., Zhao, J., Roy, A., Bates, P., Aslanidi, O. Toward patient-specific prediction of ablation strategies for atrial fibrillation using deep learning. *Front. Physiol.* 12:674106, 2021, doi: 10.3389/fphys.2021.674106.

Address for correspondence:

Dr Oleg Aslanidi
Department of Biomedical Engineering
King's College London, St Thomas' Hospital
London SE1 7EH, United Kingdom
oleg.aslanidi@kcl.ac.uk